Chapter 8

Indirect Antiproton Observations: Electron Damping

For the first time, the unique two component cloud consisting of antiprotons and electrons can be non-destructively studied in a Penning trap. Unlike the case with another ion species mixed with protons (Chapter 7), the companion electrons are much less massive and synchrotron radiation removes cyclotron energy with a time constant of approximately 0.1 seconds. During the initial loading and cooling studies only the axial preamplifiers (for $\nu_z(e^-)$ and $\nu_z(\overline{p})$) were connected to the trap. The electrons aid in the cooling of the antiprotons during resonance measurements. Using electron damping, we have performed a preliminary mass comparison of $m_{\overline{p}}/m_e$.

8.1 Observations via Axial Heating of Electrons and Antiprotons

Non-destructive observations of the antiproton cyclotron frequency are obtained using indirect collisional coupling to the axial motion of either the electrons or the antiprotons. We monitor the square law voltage developed across the axial resonant circuits at $\nu_z(e^-)$ and $\nu_z(\overline{p})$ in a finite bandwidth (typically 1 to 3 kHz) as a function of antiproton cyclotron heating. Heated antiproton axial signals are not easily observable immediately after loading and cooling when the trapped electron number still significantly outnumbers the antiprotons. When the electron number

is sufficiently reduced by the drive and dip methods described in Section 4.3, the electrons are often no longer resolved as a dip in the noise spectra. However, if either the antiprotons or electrons are heated, the heated motion can be detected using the tuned circuits in a fashion analogous to the proton bolometric technique.

When the antiprotons are driven resonantly at their cyclotron frequency, we observe axial heating of both electrons and antiprotons as shown in Fig. 8.1(a) and (b). When the resonant heating drive is turned off, both of the heated signals decay with the same time constant, presumably the time required to transfer energy from the antiprotons to the electrons which then cool much more rapidly. The antiproton damping time constant (for a fixed drive strength), typically ranges between 1 and 1000 seconds depending upon particle numbers and spatial overlap. Figure 8.1(a) and (b) shows the best resolution that we achieved by the careful control of the heat input, and by sweeping very slowly. Electrons are still present as observed by the heating of the electron axial signal. Figure 8.1(c) shows the resulting square law output as a function of cyclotron heating when too much heat or too few electrons are in the trap. If insufficient electrons remain in the trap, we observe no heated electron signal at $\nu_z(e^-)$ and the antiprotons can remain heated for many hours. With such little damping it is difficult to make a return sweep that can give the 'crossing' signature of the cyclotron resonant frequency.

8.2 Preliminary Mass Comparison

By performing a series of indirect cyclotron measurements on this mixed system we have made preliminary mass comparison. To measure the antiproton cyclotron frequency, the trapping potential is adjusted to $V_1 \approx 71$ Volts for which the maximum axial antiproton signal resulting from the heated cyclotron motion is observed at the frequency $\nu_z(1)$. The square law signal is then monitored as the antiproton cyclotron drive is swept slowly upward and downward through resonance. The free space antiproton cyclotron frequency (2.12) is

$$\nu_c(1) = \nu_c'(1) + \frac{(\nu_z(1))^2}{2\nu_c'(1)}. \tag{8.1}$$

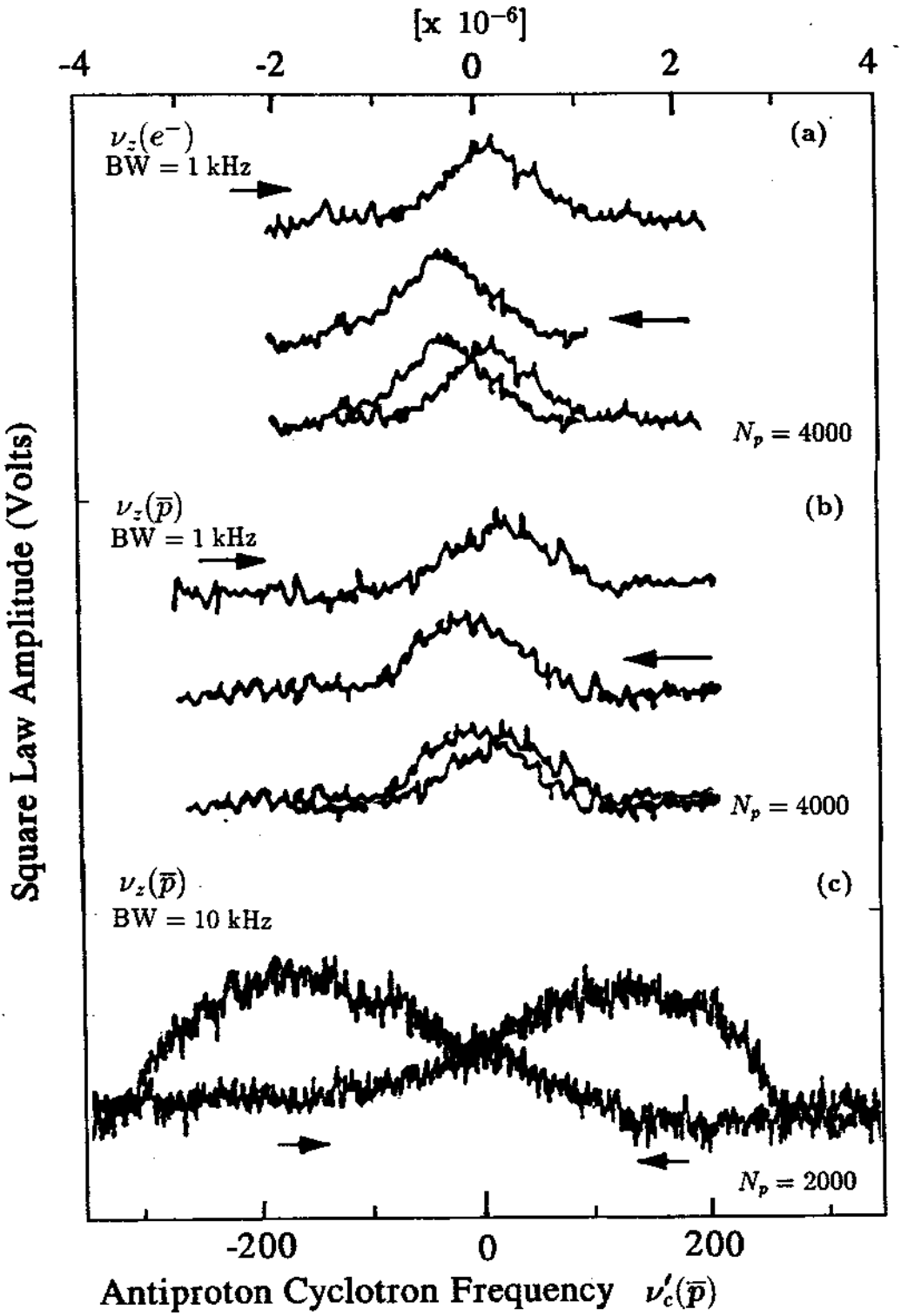

Figure 8.1: Detected axial heating of the electrons (a) and antiprotons (b) as a function of driving on the antiproton cyclotron frequency $\nu_c'(\overline{p})$. (c) The resulting axial antiproton signal resulting from either increased cyclotron drive power or reduced number of electrons.

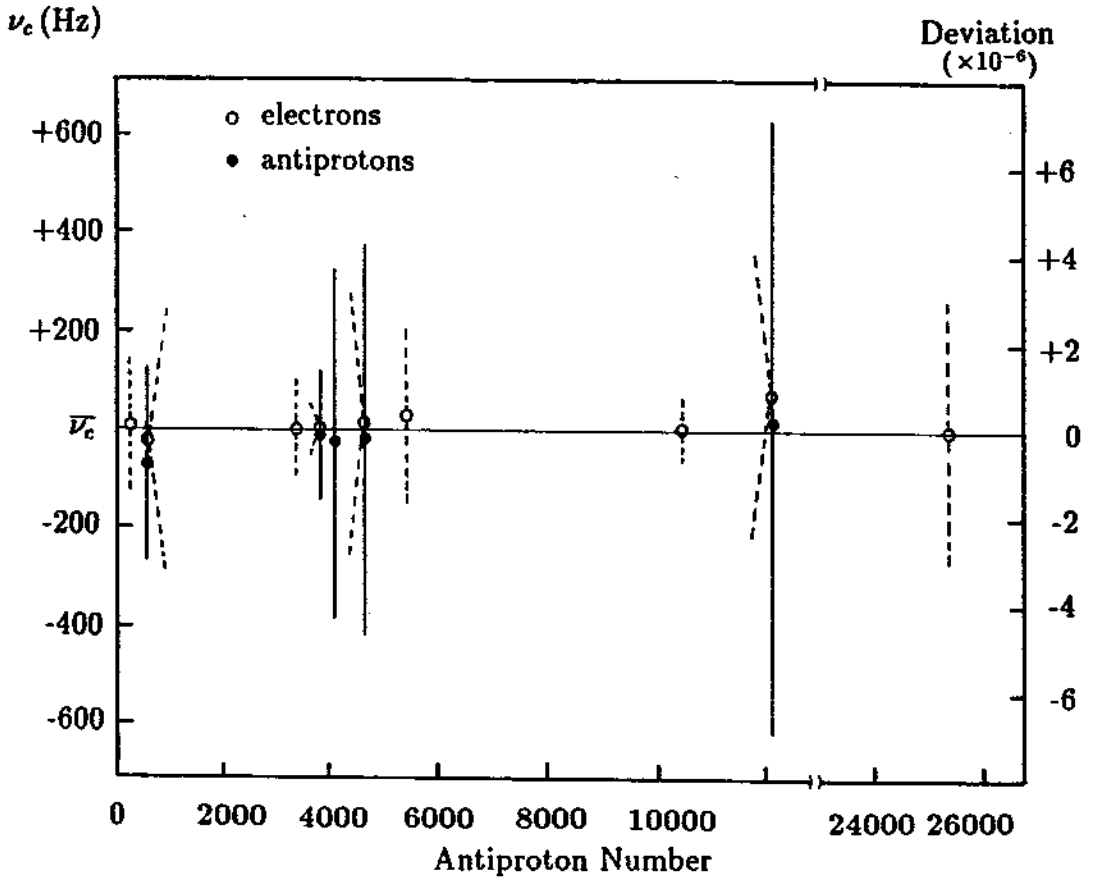

Figure 8.2: Antiproton cyclotron frequency as a function of antiproton number as measured through the axial heating of both antiprotons and electrons by collisional coupling.

Similarly, the trapping potential is adjusted to a new value $V_2 \approx 32$ Volts so that the electrons are resonant with their tuned circuit. The heated electron signal is monitored as the antiproton heating drive is again swept upward and downward through resonance at the cyclotron frequency $\nu_c'(2)$ which is different from $\nu_c'(1)$ because of the different trapping potential. This gives a second free space cyclotron frequency *for* the antiproton but measured ***using*** the electron expressed as

$$\nu_c(2) = \nu_c'(2) + \frac{\nu_z^2(1)}{2\nu_c'(2)}\frac{V_1}{V_2}. \tag{8.2}$$

In Fig. 8.2 we show that the measured cyclotron frequency does not shift when the antiproton number is varied by 2 orders of magnitude. In all cases, the measured cyclotron frequencies as observed through the antiproton heating or the electron heating agree. We use the total heated linewidth as the uncertainty since the lineshape is not well understood though much of the hysteresis results from the damping time of the antiprotons.

By performing cyclotron measurements on small clouds of electrons as described in Chapter 6, a mass comparison of antiprotons to electrons is made. A comparison of cyclotron frequencies gives

$$\frac{\nu_c(e^-))}{(\nu_c(\overline{p}))_w} = 1836.1534(16), \tag{8.3}$$

where we have taken the weighted average of the antiproton data shown in Fig. 8.2. Using the best value for the proton-electron mass ratio by VanDyck et.al.[100,72]

$$\frac{m_p}{m_e} = 1836.152\ 701(37) \tag{8.4}$$

we infer the antiproton to proton mass ratio to be:

$$\frac{\nu_c(e^-)}{\nu_c(\overline{p})}\left(\frac{m_{e^-}}{m_p}\right) \Rightarrow \frac{m_{\overline{p}}}{m_p} = 1.000\ 000\ 35(87). \tag{8.5}$$

Even with the indirect technique of detecting the antiproton cyclotron frequency, this fractional uncertainty of 8.7×10^{-7} is nearly 60 times more accurate than inferred from exotic atom methods.

The precision and accuracy of this technique are limited in two ways. First, since we observe axial heating in a relatively large bandwidth, the precision of the

correction $\nu_z^2/2\nu_c'$ is limited by our inability to identify a precise axial frequency. Second, shifts in the axial and cyclotron frequency are observed when too much heat is put in the system. Such shifts, which can be many parts in 10^6, most likely result from the large spatial extent of the cloud and the sampling of field imperfections. Substantial particle heating results from the strong cyclotron drives used to transfer energy to the axial motion by predominantly collisional mechanisms. For more precise and accurate measurements the perturbations resulting from such large amounts of resonant heating will be prohibitive.